

N^* decays to $N\omega$ from new data on $\gamma p \rightarrow \omega p$

I. Denisenko^a, A.V. Anisovich^{a,b}, V. Crede^c, H. Eberhardt^d, E. Klempt^a, V.A. Nikonov^{a,b},
A.V. Sarantsev^{a,b}, H. Schmieden^d, U. Thoma^a, A. Wilson^a

^a*Helmholtz-Institut für Strahlen- und Kernphysik der Universität Bonn, Germany*

^b*Petersburg Nuclear Physics Institute, Gatchina, Russia*

^c*Department of Physics, Florida State University, Tallahassee, USA*

^d*Physikalisches Institut der Universität Bonn, Germany*

Abstract

Data on the reaction $\gamma p \rightarrow \omega p$ with $\omega \rightarrow \pi^0 \gamma$, taken with unpolarized or polarized beams in combination with an unpolarized or polarized proton-target, were analyzed within the Bonn-Gatchina (BnGa) partial wave analysis. Differential cross sections, several spin density matrix elements, the beam asymmetry Σ , the normalized helicity difference E , and the correlation G between linear photon and longitudinal target polarization were included in a large data base on pion and photo-induced reactions. The data on ω photoproduction are used to determine twelve $N^* \rightarrow N\omega$ branching ratios; most of these are determined for the first time.

PACS: 11.80.Et, 13.30.-a, 13.40.-f, 13.60.Le

Submitted: June 17, 2021

1. Introduction

The interaction of real or virtual photons with protons at high energies - as studied extensively at HERA for masses up to 250 GeV [1] - is successfully described as a diffractive process. The photon converts into a vector meson (ρ^0 , ϕ , ω) of the same quantum numbers $J^{PC} = 1^{--}$, i.e. of identical spin, parity, and charge parity. The vector meson then scatters off the proton by the exchange of Pomerons, virtual color- and flavorless objects carrying the quantum numbers of the vacuum [2, 3]. A detailed comparison of the photoproduction of ρ^0 , ϕ , and ω mesons reveals, however, that for ω photoproduction at intermediate energies, $E_\gamma < 5$ GeV, Pomeron exchange is no longer sufficient to reproduce the data, and it has been suggested that pion and f_2 exchange become the dominant contributions [4].

At lower energies, close to the ω production threshold, N^* resonances are likely to contribute to the reaction. The SAPHIR collaboration reported differential cross sections and spin density matrix elements in the center-of-mass energy range from the ω production threshold to 2.4 GeV [5]. The authors concluded that in this mass range diffraction is no longer dominant, and that resonance formation must play an important role. GRAAL data on this reaction confirmed the need for resonances to understand the dynamics of ω photoproduction [6]. The CBELSA/TAPS collaboration reported large photon asymmetries which indicated s-channel resonance formation on top of t-channel exchange processes [7]. The CLAS collaboration reported

a high-statistics study of ω photoproduction and analyzed the data with a partial-wave-analysis model [8, 9]. Differential cross sections and spin density matrix elements were described with reasonable accuracy when several resonances were introduced: $N(1680)5/2^+$ and $N(1700)3/2^-$ near threshold and at least one higher-mass state, $N(2190)7/2^-$. Suggestive evidence was reported for the presence of a $J^P = 5/2^+$ state around 2 GeV. The $J^P = 3/2^+$ wave was reported to have a complicated structure, possibly with two close-by resonances in the 1.9 GeV region. Recently, photoproduction of ω mesons off the proton was studied by the A2 Collaboration at MAMI, and differential cross sections were presented from threshold to $E_\gamma = 1.4$ GeV with 15-MeV binning and full angular coverage [10]. No resonant contributions were discussed.

Partial wave analyses confirmed the need for nucleon excitations to describe photoproduction of ω mesons. Qiang Zhao [11] used an effective Lagrangian and found that $N(1720)3/2^+$ and $N(1680)5/2^+$ dominate the reaction. Predictions of Capstick and Roberts [12] were used in [13] to calculate the ω photoproduction cross section. The resonant contributions were shown to have a significant impact on the predictions. Titov and Lee [14] applied an effective Lagrangian approach to study the role of the nucleon resonances in ω photoproduction at energies near the threshold and found that their contribution is very significant. In a pioneering coupled-channel analysis, Penner and Mosel [15] fitted data on pion and photo-induced reactions including $\pi^- p \rightarrow \omega n$ [16, 17, 18, 19] and $\gamma p \rightarrow \omega p$ [5] and determined first $N^* \rightarrow N\omega$ branching ratios. In

a coupled-channel analysis including further data, Shklyar *et al.* [20] found strong contributions from $N(1680)5/2^+$ and $N(1675)5/2^-$ to the $\gamma p \rightarrow \omega p$ reactions.

In this letter we report on a partial wave analysis of ω photoproduction of data taken recently at the Bonn *ELectron Stretcher Accelerator* ELSA. We restrict the analysis on data from the CBELSA/TAPS experiment; a discussion of discrepancies between different data sets and the data dependence of the results will be presented elsewhere [21]. CBELSA/TAPS data on the differential cross section and on the Spin-density Matrix Elements (SDMEs) were reported in [22]: ρ_{00} , ρ_{10} , ρ_{1-1} for unpolarized incident photons, and ρ_{00}^1 , ρ_{11}^1 , ρ_{1-1}^1 , ρ_{10}^2 , ρ_{10}^2 , ρ_{1-1}^2 for linearly polarized photons. Differential cross sections and SDMEs cover the photon energy range from 1150 to 2500 MeV; the SDMEs for polarized incident photons are restricted to $E_\gamma < 1650$ MeV. The SDMEs describe the polarization state and the polarization transfer of the γp system to the final state. Results on the beam asymmetry Σ with respect to the ω direction and with respect to the direction of the π^0 from $\omega \rightarrow \pi^0 \gamma$ (Σ_π) are taken from [7]. In [23], the helicity asymmetry $E = (\sigma_{1/2} - \sigma_{3/2}) / (\sigma_{1/2} + \sigma_{3/2})$ was presented for the photon energy range from 1108 to 2300 MeV; the correlation between linear photon polarization and transverse target polarization (G and G_π) was given for one bin in photon energy covering 1108 to 1300 MeV.

2. Data from CBELSA/TAPS on $\gamma p \rightarrow \omega p$

The differential cross sections, separated into 50 MeV wide bins in incoming photon energy and 24 angular bins, are shown in Figure 1. The distributions show a strong forward peaking, in particular at higher energies: diffractive production of ω mesons plays a role which becomes increasingly important with increasing photon energy. These and the other CBELSA/TAPS data are compared with the results of a partial wave analysis (PWA) fit described below.

The results on Σ and Σ_π are compared to the PWA fit in Fig. 2. The results have been reported earlier [7]. For the measurement of E (G), circularly (linearly) polarized photons and longitudinally polarized protons were used. Data selection and analysis are documented in [23]. Here, the results on G and G_π are shown in Fig. 2 and those on E in Fig. 3. The results are compared to the PWA fit.

A selection of unpolarized SDMEs ρ_{00}^0 , ρ_{1-1}^0 , and $Re\rho_{10}^0$ is shown in Figure 4. The events were divided into 11 equally distributed angular bins. Also shown in Figure 4 are selected SDMEs measured with linearly polarized photons (ρ^1 and ρ^2): They were extracted but now considering the polarization. Due to the increased number of fit parameters (SDMEs) and the low statistics, the number of angular bins was reduced to four equally sized bins. The statistical uncertainties were estimated by considering a large array of toy Monte Carlo generated data sets of different sizes and polarization degrees. The systematic uncertainties were found by considering experimental

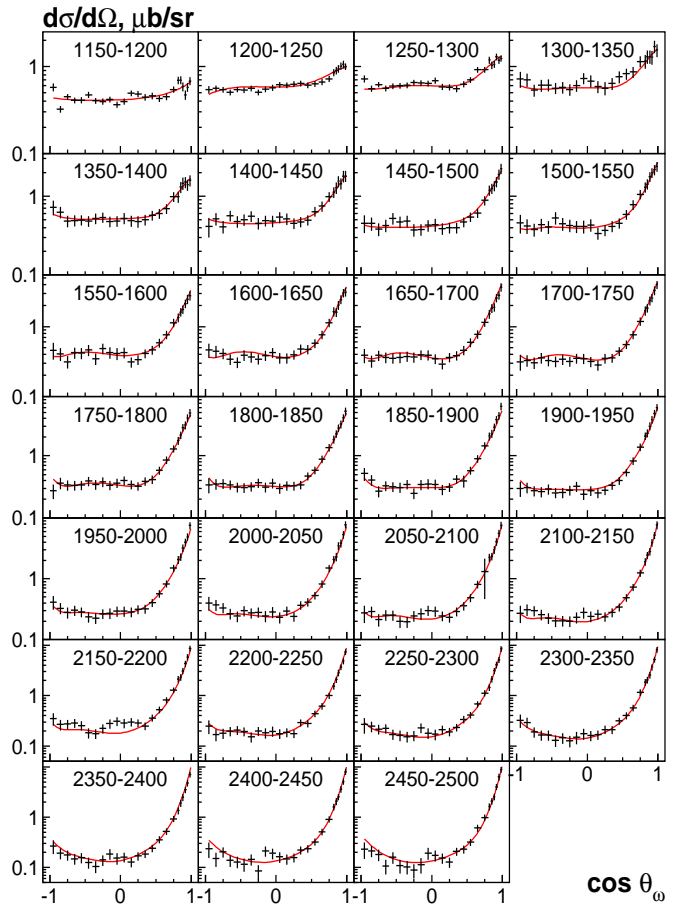


Figure 1: (Color Online) Differential Cross Sections for $\gamma p \rightarrow p\omega$ from the CBELSA/TAPS experiment in bins of the photon energy (in MeV) [22]. The total uncertainty for each data point – calculated from the squared sum of statistical and systematic errors – is represented as a vertical bar. The solid line is the PWA fit to the data.

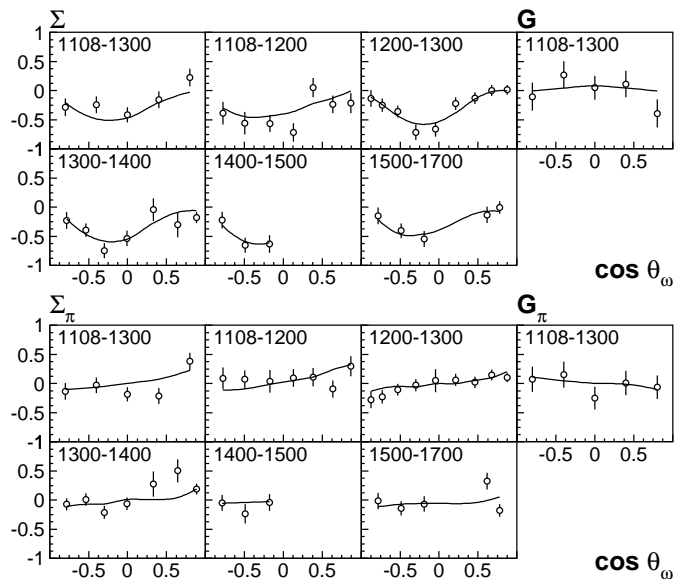


Figure 2: The beam asymmetry Σ (with respect to ω direction) or Σ_π (with respect to the direction of the π^0 from the $\omega \rightarrow \pi^0 \gamma$ decay) in bins of the photon energy [7]. The results on G , G_π are from [23].

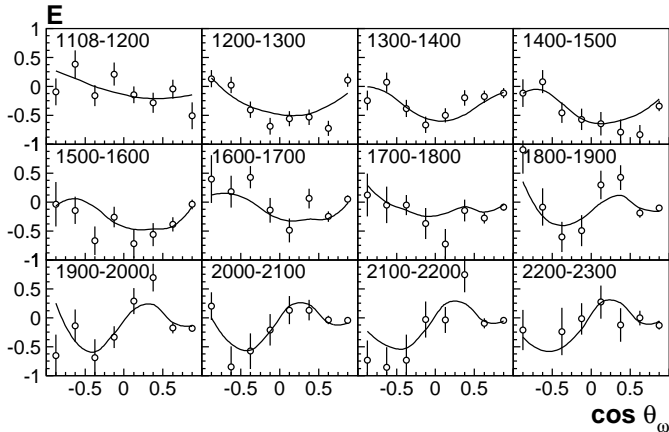


Figure 3: The helicity asymmetry E in bins of the photon energy [23].

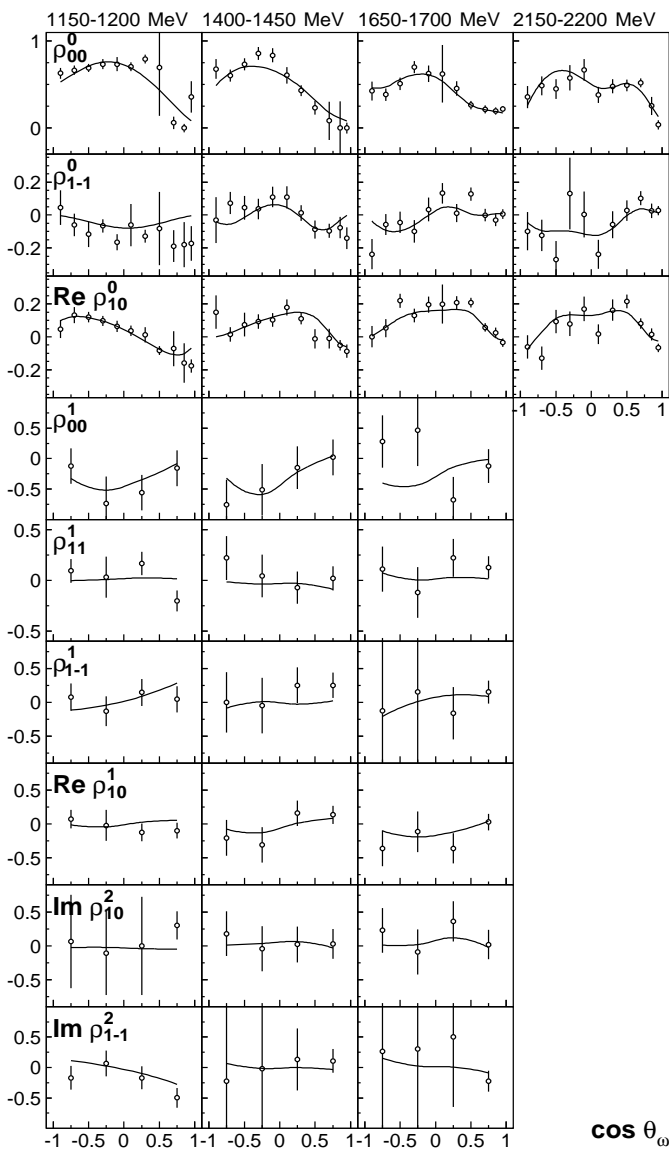


Figure 4: (Color Online) Spin Density Matrix Elements in the Adair frame from the CBELSA/TAPS experiment for selected bins of the photon energy (in MeV) [22]. The total uncertainty for each data point represented as a vertical bar. The solid curve represents the BnGa PWA solution.

analysis uncertainties, uncertainties from the Monte Carlo simulation, a possible target shift away from the nominal position, and kinematic fitting uncertainties [22]. The data not shown are fitted as well, with the same fit quality as the data shown in the figures.

3. Partial wave analysis

The data were included in the large BnGa data base covering pion and photo-induced reactions. The fit uses the dispersion relation approach based on the N/D technique which corresponds to the solution of the Bethe-Salpeter equation in the case of a separable interaction. In a simplified case when the regularization of the dispersion integral is independent from the initial and final states this method is algebraically equal to a modified K-matrix approach:

$$\hat{\mathbf{A}}(s) = \hat{\mathbf{K}} (\hat{\mathbf{I}} - \hat{\mathbf{B}}\hat{\mathbf{K}})^{-1}. \quad (1)$$

The multi-channel amplitude $\hat{\mathbf{A}}(s)$ with the matrix elements $A_{ab}(s)$ defines the transition amplitude from the K-matrix channel 'a' to the K-matrix channel 'b'. $\hat{\mathbf{B}}$ is a diagonal matrix of the respective loop diagrams with an imaginary part equal to the corresponding phase space volume:

$$\hat{B}_i = \text{Re}B_i + i\rho_i. \quad (2)$$

If the real part of the loop diagram is neglected, this method corresponds to the classical K-matrix approach.

In the present fit we used a subtraction procedure to calculate the elements of the B-matrix:

$$B_i(s) = b_i + (s - (m_{1i} + m_{2i})^2) \times \int_{(m_{1i} + m_{2i})^2}^{\infty} \frac{ds'}{\pi} \frac{\rho_i(s')}{(s' - s - i\epsilon)(s' - (m_{1i} + m_{2i})^2)} \quad (3)$$

where ϵ goes to zero. b_i are subtraction constants, and m_{1i}, m_{2i} are masses of the particles in channel i .

The K matrix elements combine the contributions from resonances and from background:

$$K_{ab} = \sum_{\alpha} \frac{g_a^{\alpha} g_b^{\alpha}}{M_{\alpha}^2 - s} + f_{ab}. \quad (4)$$

Here $g_{a,b}^{\alpha}$ are coupling constants of the pole α to the initial state a and the final state b . The number of the channels is varied for different partial waves. As a rule, it includes two-body final states $\pi N, \eta N, K\Lambda$ [24], $K\Sigma$ [25] and a number of intermediate mesonic and baryonic resonances which contribute notably to the $\gamma p \rightarrow \pi^0 \pi^0 p$ [26] and $\gamma p \rightarrow \pi^0 \eta p$ [27] cross sections. In addition, we include into the K-matrix one additional channel which describes the contribution from channels which are not taken into account explicitly. In the present solution the phase volume of inelastic channel was parametrized as the $\rho N(\omega N)$

contribution with the lowest possible orbital angular momentum.

The amplitude (1) corresponds to the sum of the tree level diagrams described by the K-matrix and diagrams with consequent rescattering due to loop diagrams (defined by the K-matrix channels) and vertices defined by the K-matrix. In the case of the photoproduction amplitude the initial γN interaction is taken into account only once and neglected in the rescattering loops due to a small coupling constant. This approach is called the P-vector approach (see e.g [28]):

$$a_b^h = P_a^h (I - BK)_{ab}^{-1} \quad \text{where} \quad (5)$$

$$P_a^h = \sum_{\alpha} \frac{A_{\alpha}^h g_a^{\alpha}}{M_{\alpha}^2 - s} + F_a.$$

Here A_{α}^h is the helicity-dependent photo-coupling of a pole α and F_a a non-resonant transition.

It is also useful to rewrite the sum of rescattering diagrams extracting the transition to the final state:

$$A_{af} = \hat{D}_{af} + [\hat{K}(\hat{I} - \hat{B}\hat{K})^{-1} \hat{B}]_{ab} \hat{D}_{bf} \quad (6)$$

$$D_{bf} = \sum_{\alpha} \frac{g_b^{(\alpha)} g_f^{(\alpha)}}{M_{\alpha}^2 - s} + \tilde{d}_{bf}. \quad (7)$$

Here $g_f^{(\alpha)}$ is the coupling of a resonance to the final state and \tilde{d}_{bf} represents the non-resonant transition from the K-matrix channel b to the final state f . If the final state corresponds to the one of the K-matrix channels, the amplitude (6) will be the same as the amplitude (1). However, this expression allows us to describe the transition to weak channels.

In cases where both, initial and final coupling constants, are weak we use an approximation which we call PD-vector. In this case the amplitude is given by

$$A_f = \hat{G}_f + \hat{P}_a [(\hat{I} - \hat{B}\hat{K})^{-1} \hat{B}]_{ab} \hat{D}_{bf}. \quad (8)$$

\hat{G}_f corresponds to a tree diagram for the transition from initial channel (γN in the case photoproduction) to the state 'f':

$$G_f = \sum_{\alpha} \frac{g_{\gamma N}^{(\alpha)} g_f^{(\alpha)}}{M_{\alpha}^2 - s} + \tilde{h}_{(\gamma N)f}. \quad (9)$$

Here, the elements $\tilde{h}_{(\gamma N)f}$ represent the direct non-resonant transitions from the initial photon-nucleon system to the different final states. These are the only new parameters of the fit once the P-vector and D-matrix are known. In the present analysis we did not introduce this non-resonant transition; instead we included reggeized pion and Pomeron exchange amplitudes. These are represented by the exchange of a Reggeon [29] in the form

$$A = g(t)R(\xi, \nu, t) \quad \text{where} \quad (10)$$

$$R(\xi, \nu, t) = \frac{1 + \xi \exp(-i\pi\alpha(t))}{\sin(\pi\alpha(t))} \left(\frac{\nu}{\nu_0} \right)^{\alpha(t)}.$$

We use $g(t) = g_0 \exp(-bt)$ as vertex function and form factor. $\alpha(t)$ describes the trajectory, $\nu = \frac{1}{2}(s - u)$, ν_0 is a normalization factor, and ξ the signature of the trajectory. Pion and Pomeron exchange both have a positive signature and therefore [30]:

$$R(+, \nu, t) = \frac{e^{-i\frac{\pi}{2}\alpha(t)}}{\sin(\frac{\pi}{2}\alpha(t))} \left(\frac{\nu}{\nu_0} \right)^{\alpha(t)}. \quad (11)$$

To eliminate the poles at $t < 0$, additional Γ -functions are introduced in (11).

$$\sin\left(\frac{\pi}{2}\alpha(t)\right) \rightarrow \sin\left(\frac{\pi}{2}\alpha(t)\right) \Gamma\left(\frac{\alpha(t)}{2}\right). \quad (12)$$

The pion and Pomeron trajectories were taken with the standard parameterization:

$$\pi \quad \alpha(t) = -0.25 + 0.85(\text{GeV}^{-2})t \quad (13)$$

$$\text{Pomeron} \quad \alpha(t) = 0.26 + 0.85(\text{GeV}^{-2})t \quad (14)$$

where t should be given in GeV^2 .

The amplitude in the form of eq. (9) is very suitable for the description of reactions with a relatively small cross section. In this case the new parameters describing the decay of resonances into the new channel or the non-resonant transitions do not influence the description of other reactions. For example, in the case of one resonance, the amplitude (9) corresponds to a relativistic Breit-Wigner amplitude with production and decay couplings in the numerator and a resonance width formed by the K-matrix channels.

4. Fit results

The fit with only the t-channel exchange amplitudes demonstrates clearly the importance of the matrix-density data and of the polarization observables. For example, a fit with only Pomeron exchange reproduces well the differential cross section above 2000 MeV, but predicts vanishing ρ_{00} density matrix elements, a vanishing beam asymmetry, a vanishing helicity asymmetry, and a vanishing G -observable. A fit which includes Pomeron and pion exchanges predicts ρ_{00} and the beam asymmetry to be very close to zero.

In our first fits, the $N\omega$ decays were admitted for all known N^* resonances [31] above or just below the $N\omega$ threshold. The reaction was fitted using the PD-vector approach (9) which allows us to use directly solution BG2014-02 with fixed parameters. We tried about 200 different fits starting from different initial couplings. The best solution showed a large contribution from the $J^P = 3/2^+$ partial wave already just above the reaction threshold. The partial waves $J^P = 3/2^-$ and $J^P = 1/2^-$ which can couple to the $N\omega$ channel in the S -wave are considerably smaller. In the energy range considered here, the Pomeron-exchange contribution rises continuously with energy and reaches about 50% of the total cross section at $W = 2000$ MeV.

Table 1: χ^2 for the solution with the standard set of N^* resonances and for the solution where one resonance with $J^P = 1/2^-$ at about 2230 MeV is added.

$N(2230)$	$d\sigma/d\Omega$	Σ	Σ_π	$G+G_\pi$	E	ρ_{00}	ρ_{10}	ρ_{1-1}
No	0.72	0.85	1.20	0.59	1.29	1.42	1.23	1.36
Yes	0.56	0.85	1.19	0.58	1.16	1.10	1.04	1.29
N_{data}	648	36	36	10	95	297	297	297

The pion exchange contribution was found to be small, although the fit quality hardly changes if one enforces it to be up to 20% of the total cross section.

The best fit with the known N^* states provides a good description of the data for masses below 2100 MeV, and an acceptable description above. We tried to improve the description by adding Breit-Wigner resonances with different quantum numbers. The best improvement was obtained when an additional resonance was introduced with a mass above 2200 MeV. Its mass optimized around 2230 MeV; its quantum numbers are not well defined: $J^P = 1/2^-, 3/2^+, 3/2^-,$ or $5/2^+$ lead to a similar fit quality. Although the new state influences the parameters of lower mass resonances only slightly, it provides some flexibility of the fit in the lower mass region and led to a significant improvement in the description of the density matrix elements also below 2100 MeV.

Next, we investigated the stability of the solution by excluding one by one the ωN couplings of the resonances. Some couplings could be put to zero, with an almost negligible deterioration of the fit. These solutions were included in the systematic error estimation.

At the next step we included in the K-matrix those $N\omega$ channels which provided significant contributions to the partial wave (instead of treating them as PD vectors). In many partial waves, the fit just reduced the partial width of the *missing channel* in favor of the $N\omega$ channel. In some cases, however, we had to refit the whole data base to find an improved solution.

The final refit of the Bonn-Gatchina data base, with the data on $\gamma p \rightarrow \omega p$ included, produced almost the same quality of the description of the other data sets: neither pole positions or decay properties of the resonances changed significantly. However, a small tuning of all couplings allowed us to improve notably the description of the $\gamma p \rightarrow \omega p$ observables.

The K-matrix solution where a $J^P = 1/2^-$ resonance in the region 2230 MeV was admitted in the fit was taken as main solution. All other solutions were used to estimate the errors from the range of values obtained in the other fits. In Table 1 we give the breakdown of the χ^2 contributions. As an example, we show the χ^2 values when the high mass $J^P = 1/2^-$ resonance is excluded from the fit. The fit quality is very similar when the spin-parity is changed to $3/2^+, 3/2^-,$ or $5/2^+.$

Table 2 lists those resonances which have an $N\omega$ de-

Table 2: Branching ratios (B.R. in %) for N^* decays into $N\omega$. Small numbers were reported in [15]. The $\delta(\chi^2)$ values give the change in χ^2 when the $N\omega$ decay mode is excluded.

Resonance	B.R.	$\delta(\chi^2)$	Resonance	B.R.	$\delta(\chi^2)$
$N(1700)3/2^-$	22 ± 12	100	$N(1900)3/2^+$	15 ± 8 13 ± 9	70
$N(1710)1/2^+$	2 ± 2 8 ± 5	26	$N(2000)5/2^+$	18 ± 8 1 ± 1	42
$N(1720)3/2^+$	26 ± 14	105	$N(2060)5/2^-$	4 ± 3	37
$N(1875)3/2^-$	13 ± 7 20 ± 4	98	$N(2100)1/2^+$	15 ± 10	78
$N(1880)1/2^+$	20 ± 8	33	$N(2150)3/2^-$	12 ± 8	99
$N(1895)1/2^-$	28 ± 12	100	$N(2190)7/2^-$	14 ± 6	131

cay mode which yields a significant improvement of the fit quality. The table gives the branching ratios, their errors, and the change in χ^2 when the coupling of a resonance is fixed to zero. The results reported in [15] are listed as small numbers.

A few comments need to be made:

From the data on $\gamma p \rightarrow \omega p$ alone, only the products of the helicity amplitudes $A_{1/2}, A_{3/2}$ and the square root of the $N^* \rightarrow N\omega$ branching ratios are determined. The helicity amplitudes can be deduced when elastic scattering data and photoproduction of pions are included in the fits.

The comparison of our results with those of Penner and Mosel [15] shows good consistency. Only the $N\omega$ branching ratios of the $N(2000)5/2^+$ resonance are different in magnitude. However, the $N(2000)5/2^+$ resonance is difficult to observe in photoproduction, and our result is only slightly more than 2σ away from zero.

The pole positions of $N(1700)3/2^-$ is fitted to values just above the $N\omega$ threshold (at 1720 MeV), those of $N(1680)5/2^+, N(1710)1/2^+$ and $N(1720)3/2^+$ below the threshold. The $N\omega$ coupling constants of these states are non-zero, leading to a non-vanishing amplitude above the $N\omega$ threshold, and suppressing these couplings leads to a notable deterioration of the fit quality. Formally, the branching ratios would be vanishing or very small since the phase space at the nominal mass of the resonance is zero or small. Therefore, the branching ratios of Table 2 for these resonances were calculated by numerical integration over the full width of the resonance. For higher-mass resonances, the numerical integration or the usual definition of the branching ratio give nearly identical results. The $N(1900)3/2^+$ in Table 2 resonance stands for a complex of two resonances - suggested as well in [8, 9] - but only the properties of $N(1900)3/2^+$ are well defined in our fits.

The branching ratios are derived from the best ten fits which yield acceptable descriptions of the data. The spread of their results is used to define the errors. The spread is hence due to systematic uncertainties, the statistical uncertainties are small. Note that the errors can be large even in cases where the statistical significance is high.

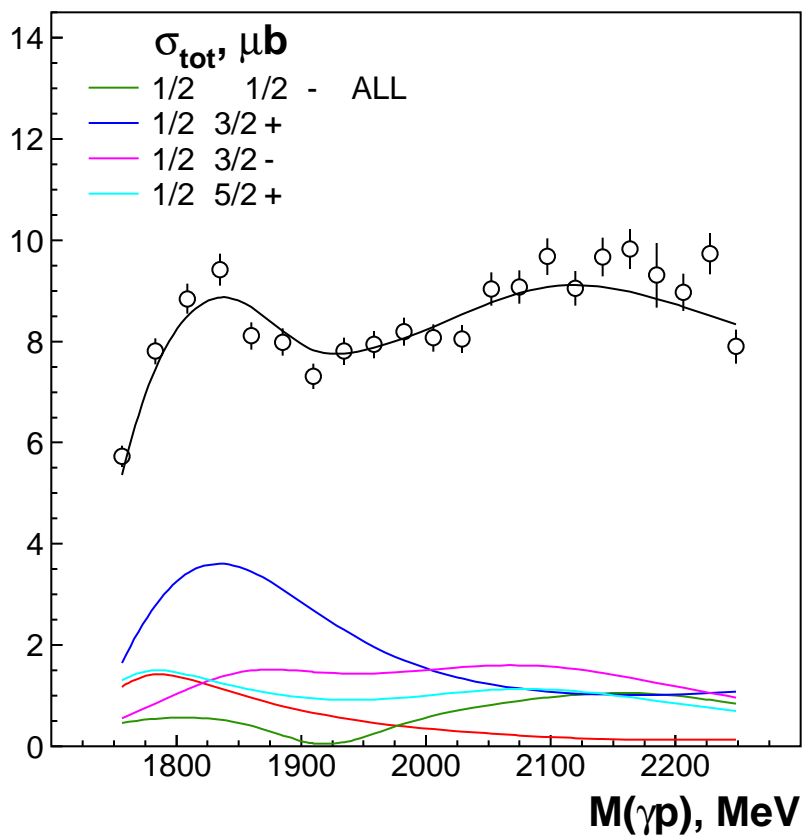
5. Summary

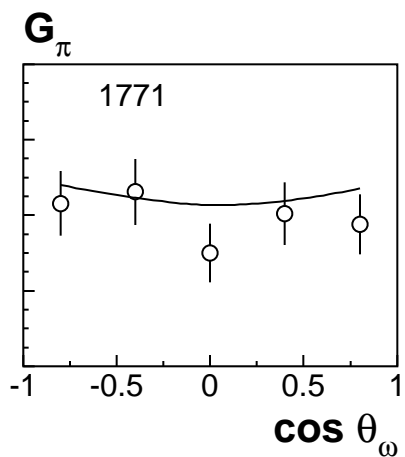
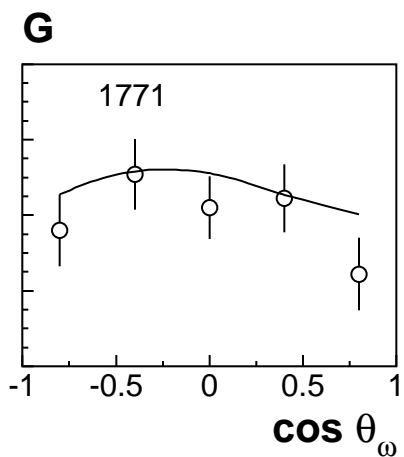
In summary, we have reported a partial wave analysis including new data on the reaction $\gamma p \rightarrow \omega p$ for unpolarized and polarized photons and unpolarized and polarized protons. The analysis is performed within the Bonn-Gatchina partial wave formalism and includes other data on pion and photo-induced reactions. Branching ratios of twelve nucleon resonances for their decay into nucleon plus ω are derived.

We would like to thank the members of the CBELSA/TAPS collaboration for letting us use their data before publication. We acknowledge support from the *Deutsche Forschungsgemeinschaft* (SFB/TR16), *Russian Foundation for Basic Research*, and *U.S. National Science Foundation*.

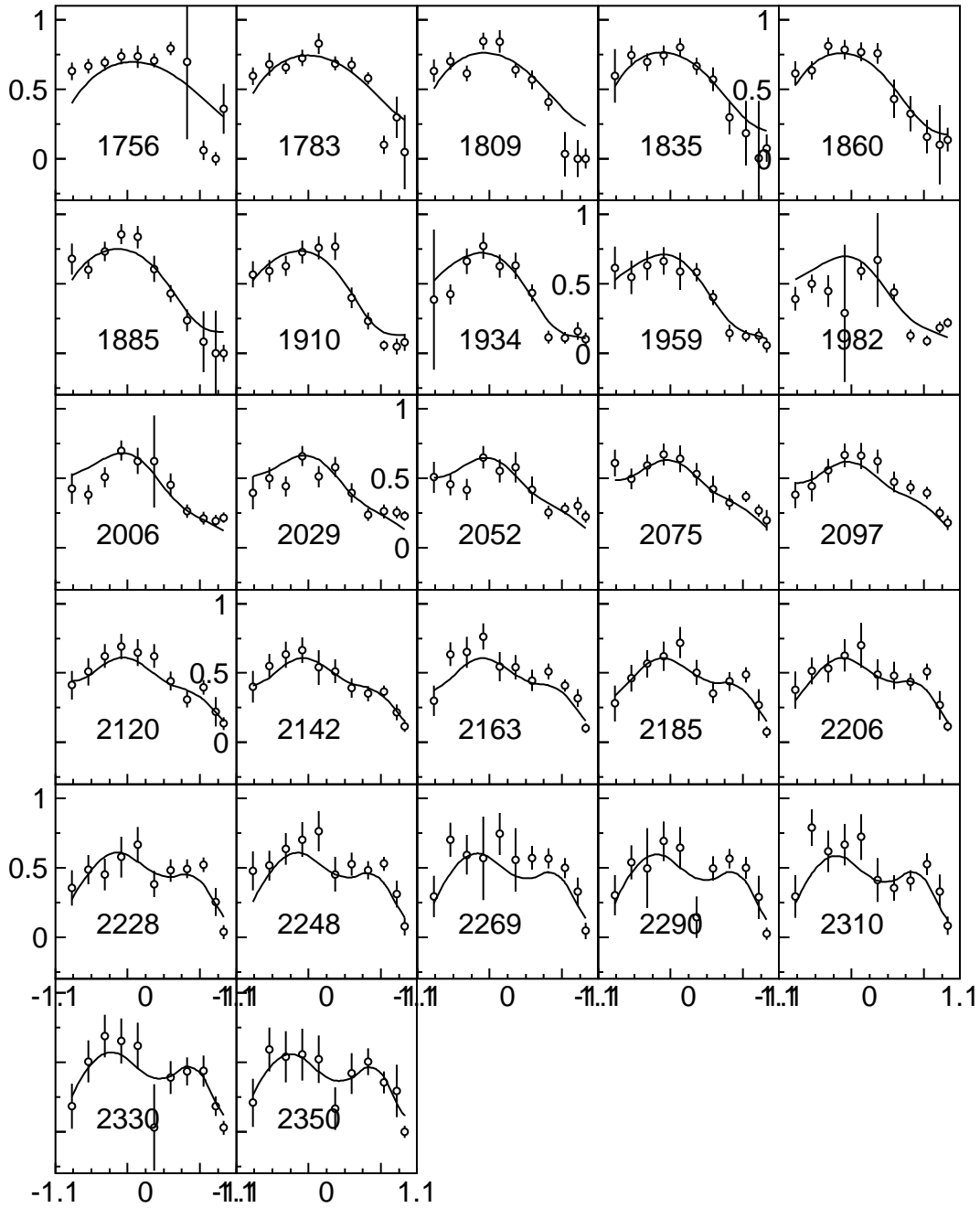
References

- [1] G. Wolf, Rept. Prog. Phys. **73**, 116202 (2010).
- [2] A. Donnachie and P. V. Landshoff, Phys. Lett. B **348**, 213 (1995).
- [3] A. Donnachie and P. V. Landshoff, Phys. Lett. B **478**, 146 (2000).
- [4] A. Sibirtsev, K. Tsushima, and S. Krewald, Phys. Rev. C **67**, 055201 (2003).
- [5] J. Barth *et al.*, Eur. Phys. J. A **18**, 117 (2003).
- [6] J. Ajaka *et al.* [GRAAL Collaboration], Phys. Rev. Lett. **96**, 132003 (2006).
- [7] F. Klein *et al.* [CBELSA/TAPS Collaboration], Phys. Rev. D **78**, 117101 (2008).
- [8] M. Williams *et al.* [CLAS Collaboration], Phys. Rev. C **80**, 065208 (2009).
- [9] M. Williams *et al.* [CLAS Collaboration], Phys. Rev. C **80**, 065209 (2009).
- [10] I. I. Strakovsky *et al.*, Phys. Rev. C **91**, no. 4, 045207 (2015)
- [11] Q. Zhao, Phys. Rev. C **63**, 025203 (2001).
- [12] S. Capstick and W. Roberts, Prog. Part. Nucl. Phys. **45**, S241 (2000).
- [13] Yongseok Oh, A. I. Titov and T. S. H. Lee, Phys. Rev. C **63**, 025201 (2001).
- [14] A. I. Titov and T. S. H. Lee, Phys. Rev. C **66**, 015204 (2002).
- [15] G. Penner and U. Mosel, Phys. Rev. C **66**, 055211 (2002).
- [16] J. S. Danburg, M. A. Abolins, O. I. Dahl, D. W. Davies, P. L. Hoch, J. Kirz, D. H. Miller and R. K. Rader, Phys. Rev. D **2**, 2564 (1970).
- [17] D. M. Binnie *et al.*, Phys. Rev. D **8**, 2789 (1973). doi:10.1103/PhysRevD.8.2789
- [18] J. Keyne *et al.*, Phys. Rev. D **14**, 28 (1976).
- [19] H. Karami *et al.*, Nucl. Phys. B **154**, 503 (1979).
- [20] V. Shklyar, H. Lenske, U. Mosel and G. Penner, Phys. Rev. C **71**, 055206 (2005) [Phys. Rev. C **72**, 019903 (2005)].
- [21] A.V. Anisovich *et al.*, *Combined partial wave analysis of $\gamma p \rightarrow \omega p$* , in preparation.
- [22] A. Wilson *et al.* [CBELSA/TAPS Collaboration], Phys. Lett. B **749**, 407 (2015).
- [23] H. Eberhardt *et al.*, Phys. Lett. B **750**, 453 (2015).
- [24] A. V. Anisovich *et al.*, Eur. Phys. J. A **48**, 15 (2012).
- [25] A. V. Anisovich *et al.*, Eur. Phys. J. A **49**, 121 (2013).
- [26] V. Sokhoyan *et al.*, Eur. Phys. J. A **51**, no. 8, 95 (2015).
- [27] E. Gutz *et al.*, Eur. Phys. J. A **50**, 74 (2014).
- [28] S. U. Chung, J. Brose, R. Hackmann, E. Klempt, S. Spanier and C. Strassburger, Annalen Phys. **4**, 404 (1995).
- [29] A. V. Sarantsev *et al.*, Eur. Phys. J. A **39**, 61 (2009).
- [30] A. Anisovich, E. Klempt, A. Sarantsev and U. Thoma, Eur. Phys. J. A **24**, 111 (2005)
- [31] K. A. Olive *et al.*, Chin. Phys. C **38**, 090001 (2014).

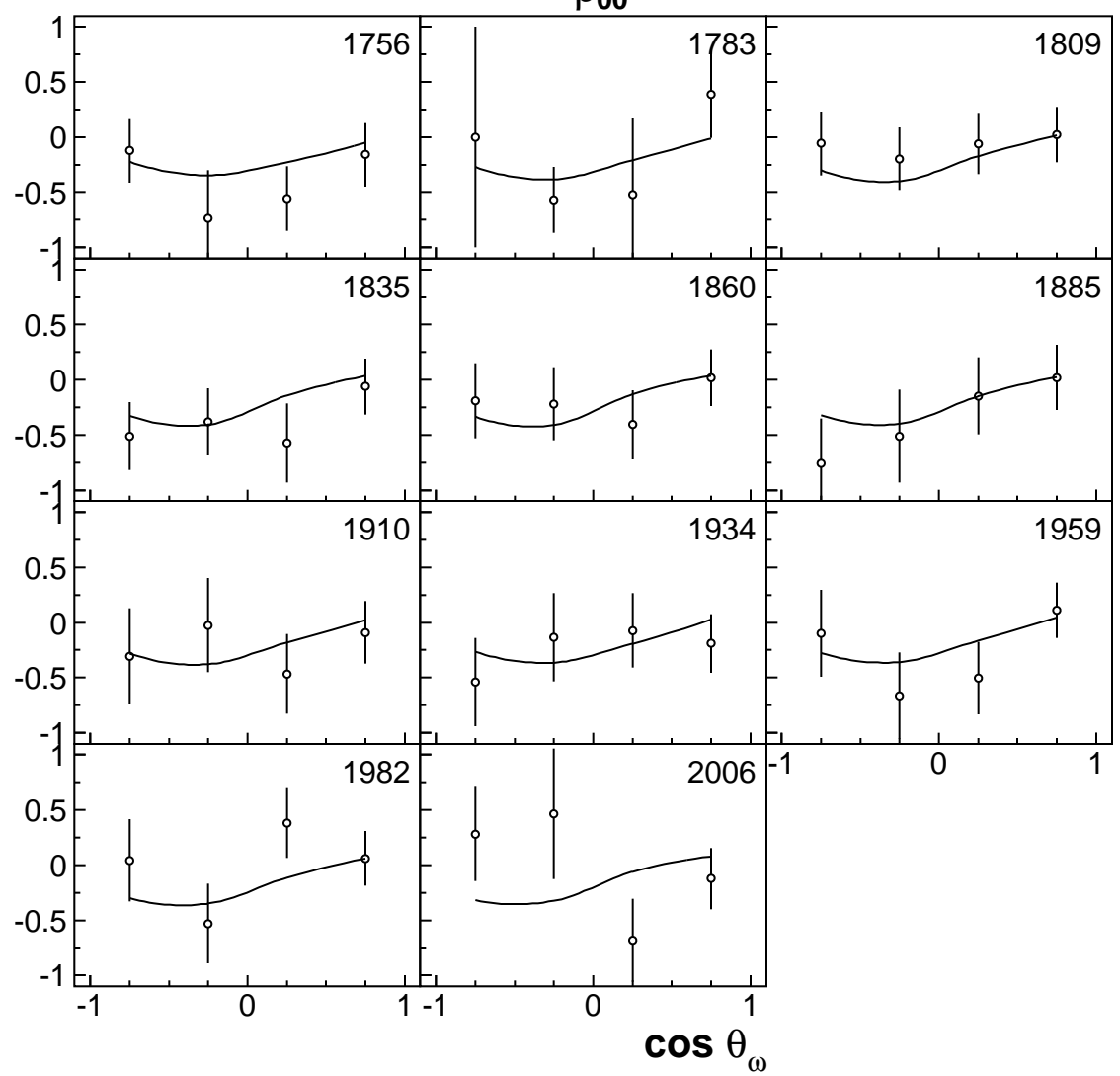




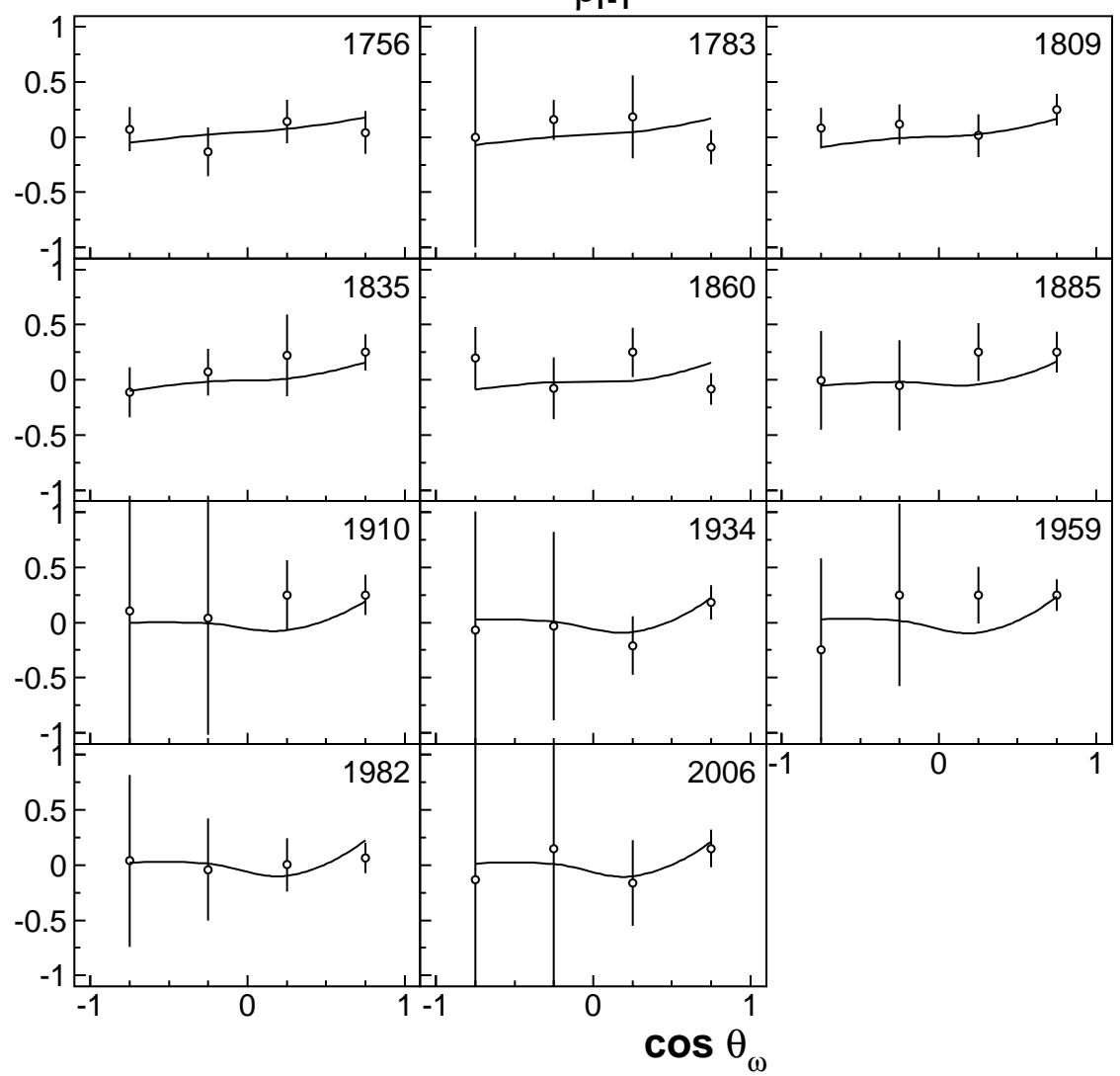
ρ_{00}

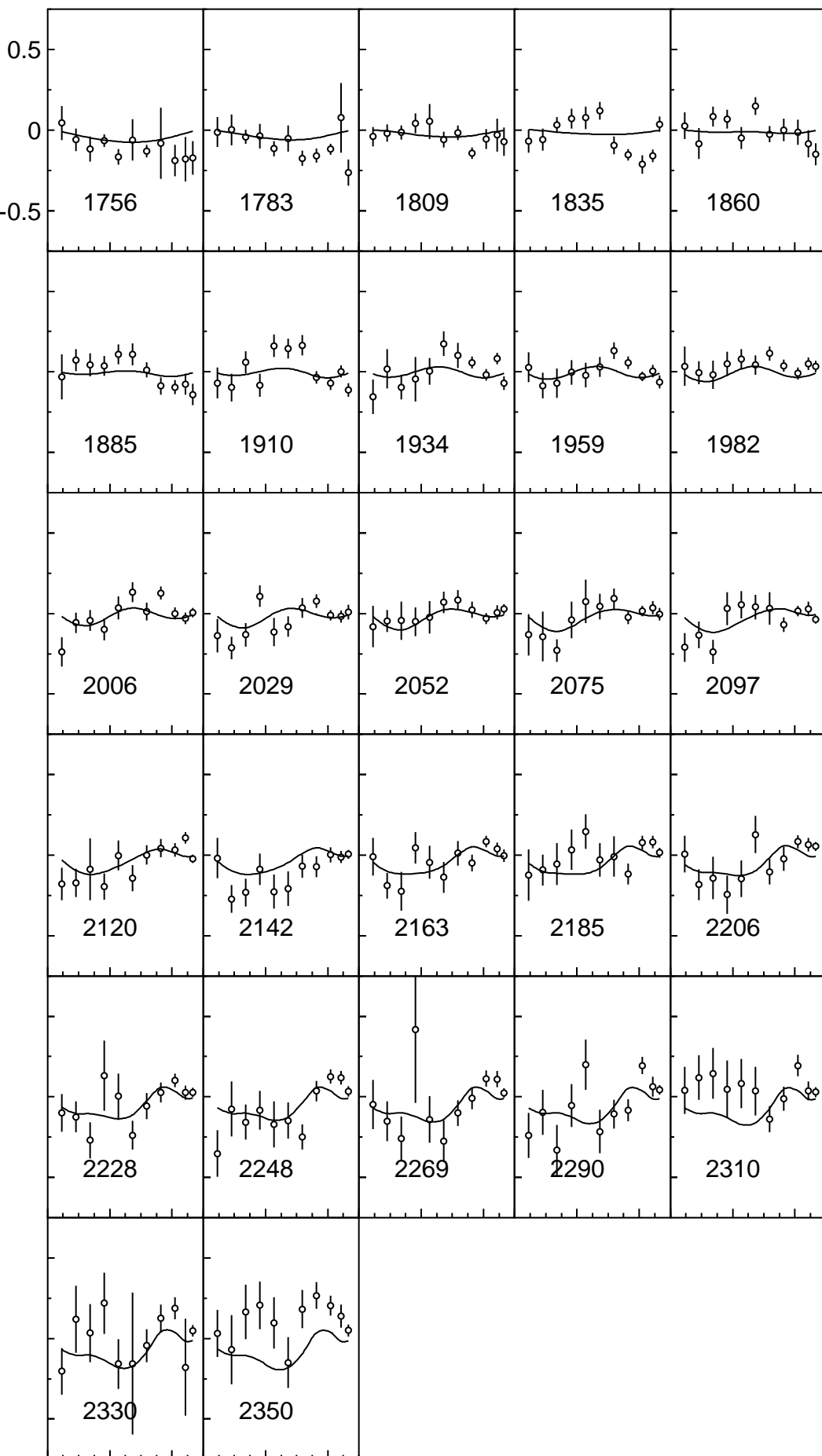


ρ_{00}^1

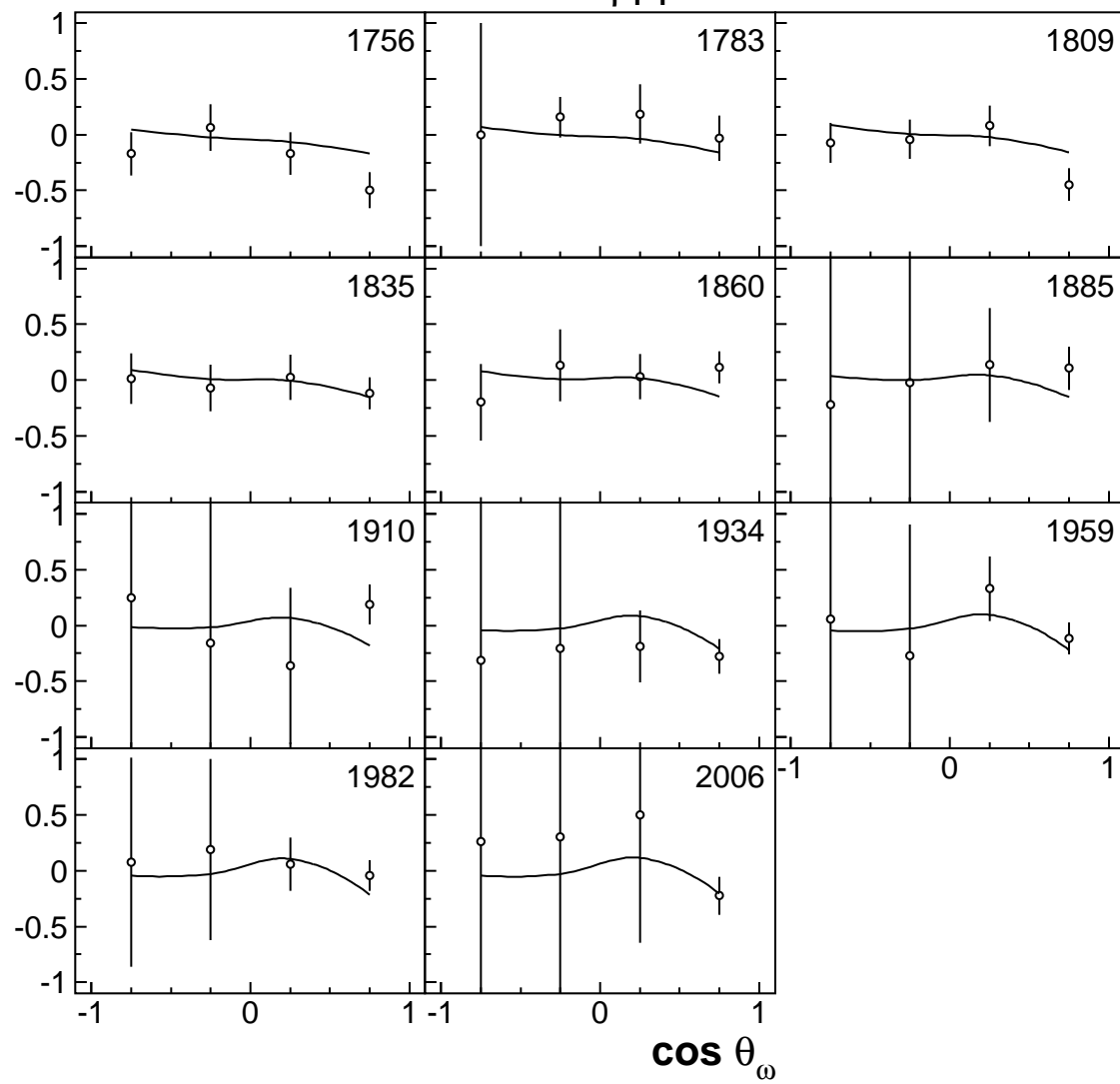


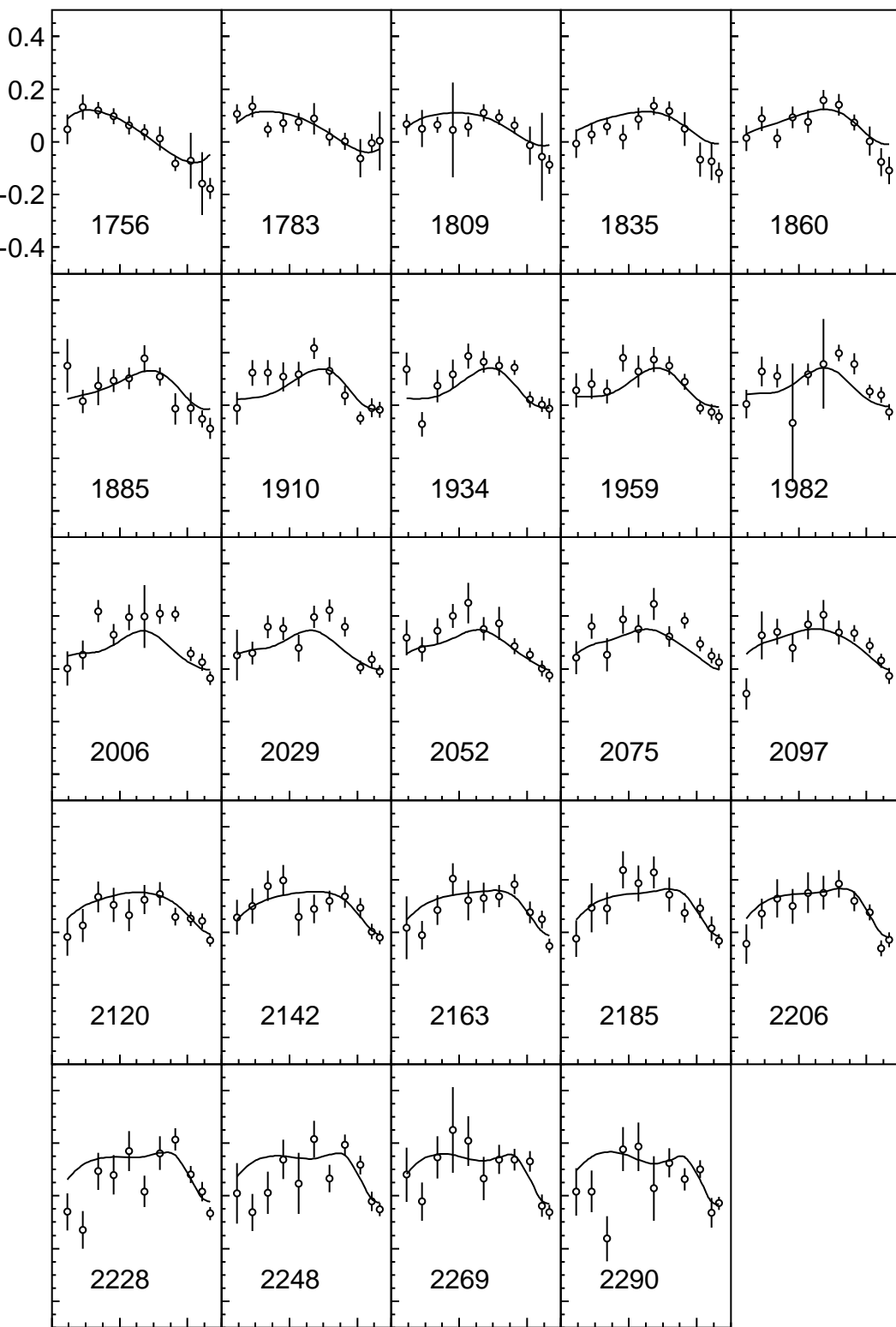
ρ_{1-1}^1





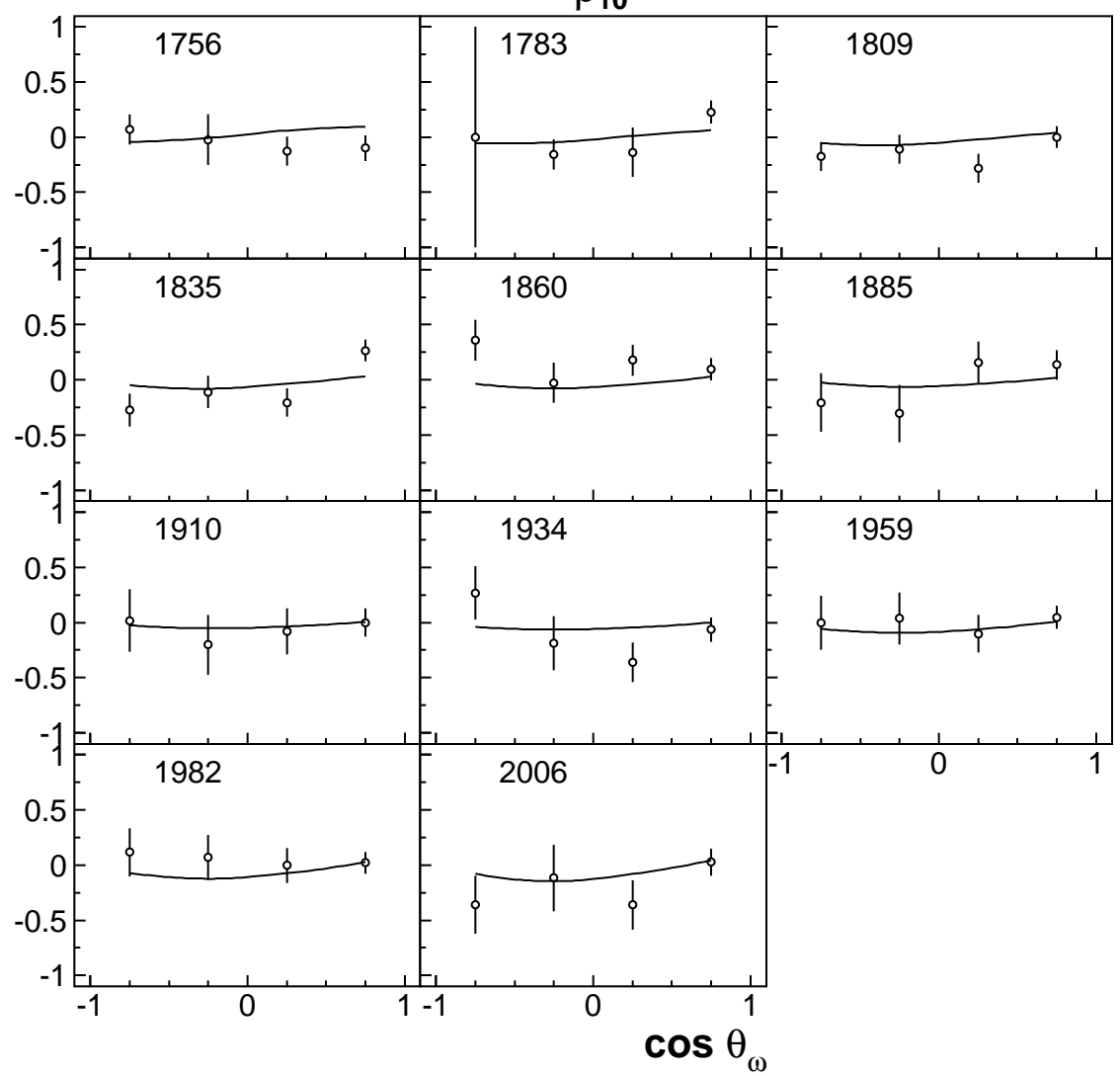
$\text{Im } \rho_{1-1}^2$



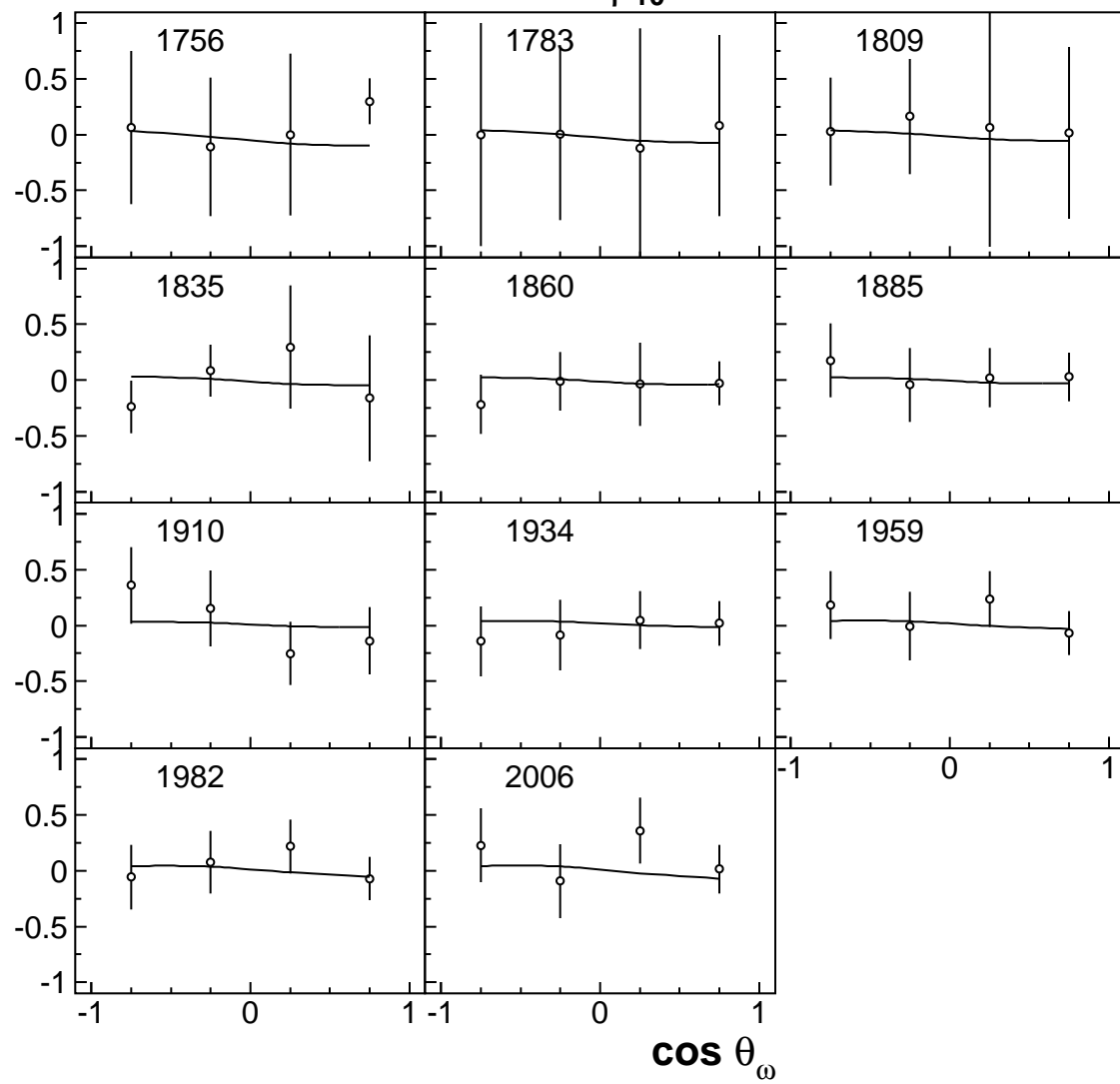


$\cos \theta_\omega$

ρ_{10}^1



$\text{Im } \rho_{10}^2$



ρ_{11}^1

